NAVAL SHIP RESEARCH AND DEVELOPMENT CENTER
Washington, D.C. 20007

TRANSIENT FLEXURAL VIBRATIONS OF SHIP-LIKE STRUCTURES EXPOSED TO UNDERWATER EXPLOSIONS

by

George Chertock

DEPARTMENT OF ACOUSTICS AND VIBRATION
RESEARCH AND DEVELOPMENT REPORT

October 1970

Report 3504

Report 3504

TRANSIENT FLEXURAL VIBRATIONS OF SHIP-LIKE STRUCTURES EXPOSED TO UNDERWATER EXPLOSIONS

The Naval Ship Research and Development Center is a U.S. Navy center for laboratory effort directed at achieving improved sea and air vehicles. It was formed in March 1967 by merging the David Taylor Model Basin at Carderock, Maryland, and the Marine Engineering Laboratory (MEL) at Annapolis, Maryland. In November 1967 the Mine Defense Laboratory (MDL), Panama City, Florida, became a part of the Center. In November 1968 MEL was redesignated as the Naval Ship Research and Development Laboratory, Annapolis, Maryland 21402 and MDL was redesignated as the Naval Ship Research and Development Laboratory, Panama City, Florida 32401.

Naval Ship Research and Development Center
Washington, D.C. 20007

NDW-NSRDC 3960/44 (Rev. 6-69)

DEPARTMENT OF THE NAVY
NAVAL SHIP RESEARCH AND DEVELOPMENT CENTER
WASHINGTON, D.C. 20034

TRANSIENT FLEXURAL VIBRATIONS OF SHIP-LIKE STRUCTURES EXPOSED TO UNDERWATER EXPLOSIONS

by

George Chertock

October 1970

Report 3504

Reprinted from THE JOURNAL OF THE ACOUSTICAL SOCIETY OF AMERICA, Vol. 48, No. 1, (Part 2), 170–180, July 1970

12.5, 12.7, 12.3

Received 20 October 1969

Transient Flexural Vibrations of Ship-Like Structures Exposed to Underwater Explosions

GEORGE CHERTOCK

Naval Ship Research and Development Center, Washington, D. C. 20034

The flexural vibrations of ship-like structures are easily excited by underwater explosions, particularly if the explosion bubble period approximately synchronizes with a period of flexural vibration. A summary of the theoretical analysis shows how the transient motions are related to the principal vibration modes of the structure, and to the distribution and history of the applied pressures. The latter depend on the size, depth, and relative position of the explosive. Experiments on small idealized ship and submarine models are described which vary the weight, depth, and position of the explosive, and which measure the instantaneous deformations of the structure with strain gauges connected into special bridge circuits to yield the normal coordinates associated with the principal flexural vibration modes. Comparison of the theory and experiments verify the theory as applied to the fundamental flexural mode, and with less precision, as applied to the higher flexural modes. The principal mode patterns and the history of the explosion bubble are verified by independent experiments.

INTRODUCTION

This paper reviews some work that was done more than 15 years ago, at what was then the David Taylor Model Basin, on the transient whipping vibrations of ships induced by nearby underwater explosions. This topic should be particularly appropriate for a session in honor of Irwin Vigness because much of his professional career was spent at a Navy laboratory investigating shock and vibration response of naval equipment to underwater explosions.

But the work under review is somewhat unique in this field of shock response, because the analysis is based on fundamental physical theory and because the theory is confirmed in detail by experiments on small and highly idealized targets. Since the theory has previously been reported in the open literature,[1] it is summarized here in general terms only. But the experiments are described in more detail, since they were originally reported in reports with very limited circulation.[2] The principal objective of the original investigation was to explore the physical mechanism by which a ship reacts to an underwater explosion. Apart from this objective, a principal purpose of the present review is to demonstrate the analytical and experimental techniques.

The specific problem is to predict the vertical bodily motions and flexural vibrations of a long slender structure such as a ship or submarine which is exposed to a nearby underwater explosion. Figure 1 shows the geometry: AB is the longitudinal axis of the target before the explosion, while $A'B'$ represents the deformed axis during the motion. We assume that the body is slender enough so that all points on the same transverse section have the same vertical displacement. The problem then is to predict the vertical displacement y as a function of the section x and the time t—and to do this *not* by scaling up the results of some small-scale model experiment but by a theoretical analysis based on the dynamic elastic properties of the ship structure and on the size and location of the explosion.

We first summarize the relevant properties of the pressure field of an underwater explosion. Then, we discuss the principal bodily and flexural modes of motion of a slender target and show how each mode is excited by the pressure field from the explosion. Finally, we describe experiments to verify the assumed pressure field, to independently establish the principal vibration modes of the target, and to verify the quantitative details of their interaction.

I. THE PRESSURE FIELD OF AN UNDERWATER EXPLOSION

An explosion is simply a chemical reaction which very quickly converts a solid mass of explosive into an equal mass and equal volume of gas at very high temperature

and pressure. When the explosion occurs under water, the gaseous products form a bubble which expands against the ambient hydrostatic pressure and subsequently pulsates with large changes in volume and pressure. Also, the bubble migrates in response to any gradient in the ambient pressure due to gravity or to other nonisotropic effects in the field.

In the structural response experiments to be discussed here, the characteristic response times of the structure were very much longer than the duration of the chemical reaction, and very much longer than the duration of the nonlinear shock wave caused by the initial kick of the explosion. Furthermore, conditions were chosen so that bubble migration would be negligible and the pressure field from the explosion would be spherically symmetric. In such cases, the shock wave can be treated as an impulsive function and the subsequent pressure field is the same as from a simple monopole sound source whose instantaneous source strength is the volume velocity $\dot{V}(t)$ of the bubble; i.e., the pressure at field point $\mathbf{r}$ is given by

$$p(\mathbf{r},t)=\frac{\rho\dot{V}_0}{4\pi r}\delta(t-r/c)+\rho\frac{\ddot{V}(t-r/c)}{4\pi r}, \tag{1}$$

where $\delta(t-r/c)$ is the delta function with retarded time as argument, $\dot{V}_0$ is the initial volume velocity and includes the effect of the nonlinear shock wave, and $\ddot{V}$ is the volume acceleration with retarded time as argument. The significant feature of this equation is that the pressures generated by the explosion depend only on the volume of the explosion bubble versus time.

Figure 2 shows the variation of bubble volume with time. The volume pulses about its equilibrium volume (at which the internal pressure is equal to the ambient hydrostatic pressure) with relatively long slow expansions and short quick contractions. It can be shown theoretically—and it is found experimentally—that the first-peak bubble volume depends only on the charge weight W and the ambient hydrostatic pressure p_H according to the equation

$$V_m=k_1W/p_H, \tag{2}$$

where the proportionality constant k_1 depends on the nature of the explosive. The bubble loses energy during the contraction phase, and so each successive peak volume is progressively smaller. The first pulsation period T_b likewise depends on the charge weight and the hydrostatic pressure level according to the equation

$$T_b=k_2W^{1/3}/p_H{}^{5/6}, \tag{3}$$

and the pulsation period likewise decreases progressively because of energy losses. When, as in Fig. 2, the volume is expressed in units of the peak bubble volume and the time in units of the first bubble period, then the relation which results is of very wide applicability. It is found experimentally that this relation is fairly independent of the composition of the explosive and even of the migration of the bubble.

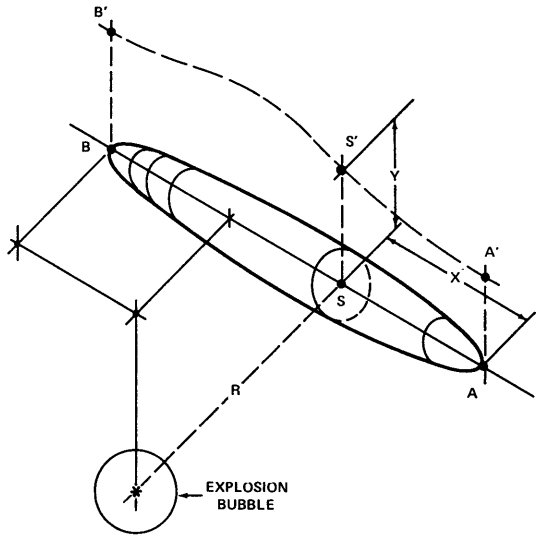

FIG. 1. Geometry of explosion bubble and submerged target.

The pressure wave generated by the explosion and by the subsequent bubble pulsation is shown in the lower part of Fig. 2. This shows the free-field pressure at a fixed distance r from the explosion center. P_s is the initial shock-wave pressure, and P_b is the bubble-pulse pressure. (Note that the drawing exaggerates the duration of the shock wave.) But the important point is that, according to Eq. 1, the curve could equally well be labelled the volume acceleration of the bubble versus time. Whenever the bubble volume exceeds the equilibrium volume, the volume acceleration is negative and the radiated pressure is negative. Whenever the bubble volume is smaller than the equilibrium volume, the volume acceleration and the radiated pressure are positive.

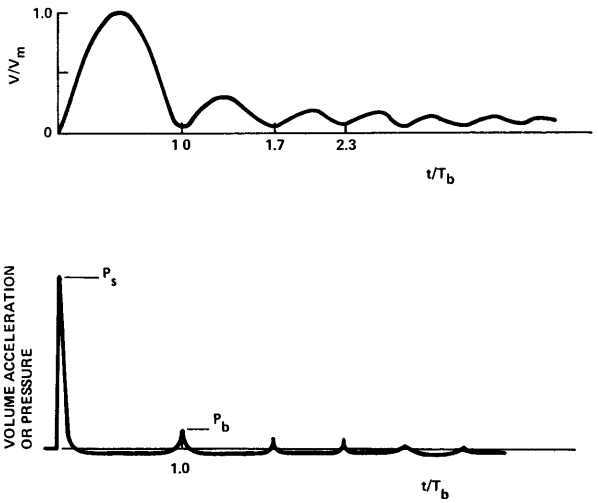

FIG. 2. Time variation of volume of explosion bubble and of pressure in water.

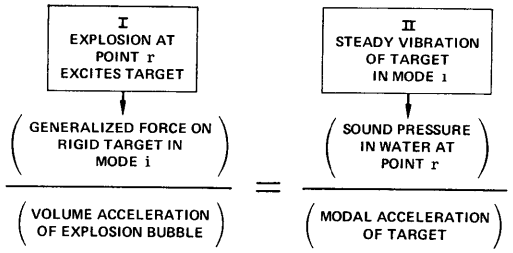

FIG. 3. Reciprocity theorem.

II. THEORETICAL ANALYSIS OF TARGET MOTIONS

The method of the analysis is the classical method of normal modes and normal coordinates. We start with the assumption that the most general dynamic configuration of the target can be written as a superposition of the normal modes of the target in *air*:

$$y(x,t)=\sum_i q_i(t)\psi_i(x);\ i=0,\ 1,\ 2,\ \cdots, \tag{4}$$

where $q_i(t)$ is a set of normal coordinates that measures the instantaneous amounts by which modes i have been excited, and $\psi_i(x)$ are a set of mode deflection patterns. It is convenient to let the subscript i denote the number of nodes in the displacement pattern along the length. Thus, ψ_0 denotes a vertical translation as a rigid body (i.e., a heaving motion of the ship), $\psi_1(x)$ denotes a rotation as a rigid body (i.e., a pitching motion of the ship), ψ_2 denotes the fundamental two-noded flexural vibration mode, ψ_3 is a three-noded flexural mode, etc. These mode shapes can possibly be determined theoretically by solving an eigenvalue problem or they can be determined experimentally by vibrating the structure. In this work it was done both ways.

Any two modes i and j are orthogonal to each other; it is convenient to normalize them so that

$$\int_0^l m(x)\psi_i(x)\psi_j(x)dx=M\delta_{ij};\ M=\int_0^l m dx, \tag{5}$$

where $m(x)$ is the mass per unit length at x, and l is the length.

But the most important property of these normal modes and normal coordinates is that the differential equation for the normal coordinate $q_i(t)$ is the equation for a linear oscillator,

$$M(\ddot{q}_i+\alpha_i^2 q_i)=Q_i(t)=-\int\int p(s,t)\psi_i(x)\cos\beta d\sigma, \tag{6}$$

where α_i is the circular resonance frequency for mode i; and where $Q_i(t)$ is the generalized force, or modal force, acting in the ith mode and is equal to an integral of a weighted pressure distribution over the surface of the target. The local pressure must be weighted in proportion to the mode function $\psi_i\cos\beta$, β being the angle between the normal to the surface and the vertical direction.

To solve this equation of motion, we must specify the local surface pressures—but their determination is complicated by the fact that they depend not only on the size and position of the explosion, but also on the shape of the target and on the motion of the target in all its modes. Hence, it is convenient to separate the pressure distribution on the surface into components as follows:

$$p(s,t)=p_{00}(s,t)+\sum_i p_i(s,t), \tag{7}$$

where $p_{00}(s,t)$ is the pressure distribution at the surface due to the explosion if the body were rigid and immovable, and p_i is the pressure distribution due solely to the motion in mode i. This decomposition is particularly useful for low-frequency motions of the ship, for then the "modal" pressures p_i at the surface are virtually the same as if the water were incompressible and the pressure were transmitted with infinite velocity. In that case, we can define an induced modal mass L_{ij} as the generalized force on the target in the ith mode, per unit acceleration of the target in the jth mode, i.e.,

$$L_{ij}=-\left[\int\int p_j(s,t)\psi_i\cos\beta d\sigma\right]\Big/\ddot{q}_j(t). \tag{8}$$

These induced modal masses, or entrained masses, or added inertias, depend only on the surface shape and the vibration patterns and are independent of the time.

In terms of these modal masses, the equation of motion for mode i becomes

$$(M_i+L_{ii})(\ddot{q}_i+\omega_i^2 q_i)+\sum_{j\neq i} L_{ij}\ddot{q}_j=-\int\int p_{00}\psi_i\cos\beta d\sigma, \tag{9}$$

where ω_i is the new circular resonance frequency in water,

$$\omega_i^2=\alpha_i^2 M_i/(M_i+L_{ii}). \tag{10}$$

The forcing function on the right of Eq. 9 is no longer coupled to the motion of the ship but still depends on the shape of the ship. But note that the motion in mode i is still coupled to all the other modes by the L_{ij} cross terms.

These cross terms vanish if there is sufficient symmetry, and in fact they are very small if the ship is sufficiently slender and uniform. But even for the general case where they do not vanish, we can show that there exists a new set of principal mode functions ψ_i' for the ship in water, a new set of resonance frequencies ω_i', and a new set of normal coordinates q_i', and that in terms of these new parameters the cross terms in the induced mass matrix *do* vanish, and the equation of motion for this new ith mode is the equation of a linear oscillator, with a single degree of freedom, and with an applied force which is completely independent of the

motion

$$M_i'(\ddot{q}_i'+\omega_i'^2 q_i')=-\int\int p_{00}\psi_i' \cos\beta d\sigma. \qquad (11)$$

The detailed theory[1] shows how to calculate these new normal modes functions ψ_i', M_i', and ω_i', but in the present application these parameters were determined experimentally.

The theoretical problem that now remains is to calculate the right-hand side of Eq. 11, which can be interpreted as the generalized force which the explosion would exert in the ith mode if the target were rigid and immovable. This can be done most easily by means of a reciprocity theorem which compares the two alternative situations of Fig. 3.

The first situation occurs when an explosion at $\mathbf{r}$ excites the target to vibrate in all its modes, and we form the ratio of $-\int\int p_{00}\psi_i \cos\beta\, d\sigma$ (the generalized force which this explosion exerts in mode i on a rigid target) to $\ddot{V}$ (the volume acceleration of the explosion bubble). The second situation occurs when we vibrate the target at its resonance frequency, by a vibration generator say, and we form the ratio of $p_i(\mathbf{r})$ (the sound pressure in the water at $\mathbf{r}$) to $\ddot{q}_i$ (the modal acceleration of the target). Then the reciprocity theorem[3] says that even though these four terms are each time dependent, their common ratio $\mu_i(\mathbf{r})$ is independent of time and depends only on the position $\mathbf{r}$ and the mode i.

Hence the forcing term in Eq. 11 can be written in this simple form

$$Q_i'=-\int\int p_{00}\psi_i' \cos\beta d\sigma=\mu_i'(\mathbf{r})\ddot{V}(t), \qquad (12)$$

where the only unknowns are the volume acceleration of the explosion bubble and the position function μ_i'. (Hereafter, we omit the primes.)

The position function μ_i may be calculated by solution of a Neumann boundary-value problem. Today we could do this by a numerical solution of an integral equation on a high-speed computer.[4] But fortunately, when this was first done[1] the computer solution was not considered, and so we obtained an approximation for μ_i which was just as accurate as a numerical solution and much more meaningful physically. In a simple form which is applicable when the mode shape in water is not too different from the mode shape in air, the position factor is given by

$$\mu_i(\mathbf{r})=-\int_0^l\left(\rho A+\frac{mL_i}{M}\right)\psi_i\frac{\partial}{\partial z}\left(\frac{1}{R}\right)dx, \qquad (13)$$

where R is the distance between the point $\mathbf{r}$ and the center of the section at x. This means that the vibrating ship acts like a line distribution of vertical dipoles, with the dipole strength per unit length depending on the local mass per unit length m, the local cross-section area A, and the local mode function $\psi_i(x)$.

The preceding analysis presupposes that the explosion and the target are both in a uniform unbounded medium. However, by use of the method of images, it is easy to modify the equations to fit the case where the target is floating, or more generally, where a free surface is nearby. The result can be most simply expressed by making the position factor for these cases be the difference between two terms. The first term is simply the position factor which would apply if the medium were unbounded. The second term is the position factor that would apply in an unbounded medium if the explosion occurred at a point $\mathbf{r}'$, which is the image of $\mathbf{r}$ in the free surface.

When the target is floating and has uniform mass per unit length and uniform section area, then the equation of motion reduces to a particularly simple form

$$\ddot{q}_i+\omega_i^2 q_i=\left[\frac{\rho A\zeta}{2\pi M}\int_0^l\frac{\psi_i dx}{R^3}\right], \qquad (14)$$

where A is the area of the underwater portion of the cross section and ζ is the depth of the charge below the free surface.

In principle, then, we now have sufficient equations to make a theoretical calculation of the whipping response of a slender ship-like body to an underwater explosion. We must separate the response into independent contributions from the principal modes of the ship in water—and separately calculate the response in each mode. To do this we must specify (by theory or by preliminary experiment) the mode shape ψ_i, resonance frequency ω_i, and position factor μ_i for each mode; also, we must specify $V(t)$, the bubble volume versus time, from the charge weight and depth. We may solve a differential equation analogous to Eq. 14, in which case it would first be necessary to calculate $\ddot{V}(t)$. Or, alternatively, we may solve a simple integral equation

$$q(t)+\omega_i^2\int_0^t\int_0^t q_i dt dt=\frac{\mu_i}{M+L_i}V(t) \qquad (15)$$

and avoid specifying the volume acceleration $\ddot{V}$.

III. EXPERIMENTS

To confirm this theoretical analysis, underwater explosion tests were made against two different targets, a floating rectangular box and a submerged cylindrical shell. Neither target was a realistic model of any ship or submarine; they were rather simple structures that were easy to analyze theoretically and easy to handle experimentally. The explosions resulted from small charges, from 1 to 8 g, at standoffs from about 1 to 5 ft. The major target motions in response to these explosions occur in the rigid-body modes, heaving and pitching. However, since the principal interest was in the elastic-

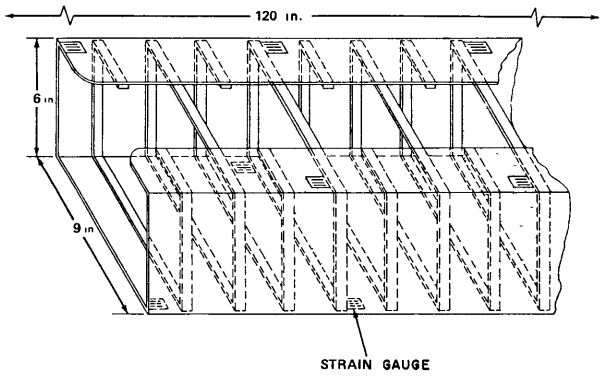

FIG. 4. Section of rectangular box target showing locations of strain gauges.

flexural modes, the target response was measured with strain gauges which do not respond to the rigid-body motions at all. The local instantaneous strain measurements in these explosion tests were converted to instantaneous measurements of a single normal coordinate $q_i(t)$ by means of relations determined in an independent series of steady vibration measurements of the target at its resonance frequency.

A. Floating Box Target

The box target was 120 in.×6 in.×9 in. as shown in Fig. 4. The shell, 48 mils thick, was strengthened by transverse bar stiffeners and ballasted with steel bars, which were bolted to each stiffener along the bottom. The box with ballast weighed 105 lb and had a draft of 2.6 in. The basic instrumentation consisted of 44 resistance-wire strain gauges, SR4 Type A1, which measured the longitudinal strains along the top and bottom. The 44 gauges were wired into 11 bridge circuits to measure the bending curvature at 11 equally spaced transverse sections along the box. The signals were detected and amplified on a multichannel carrier-type amplifier, and recorded with a multichannel galvanometer oscillograph, all with a net frequency response that was flat from dc to about 400 cps. The deflections could be measured with accelerometers at 13 sections along the target, and recorded through the same amplifying and recording equipment.

The normal-mode patterns in strain and deflection and the resonance frequencies were measured by shaking the target in air and in water by means of a commercial vibration generator attached to one end of the box. Figure 5 shows the fundamental flexure mode $\psi_2(x)$ and the bending curvatures $\psi_2(x)''$ of the box target, as measured in air and in water, and compares the results with theoretical calculations. The latter are simply the standard eigenfunctions for the bending vibration of a slender uniform rod. There is good agreement between the deflection patterns in air with those in water, and with the theoretical deflection patterns. The experimental bending strains in air or water are slightly smaller than the theoretical values for the same deflection. Figure 6 shows the deflections $\psi_3(x)$, and bending curvatures $\psi_3(x)''$ in the three-noded flexure

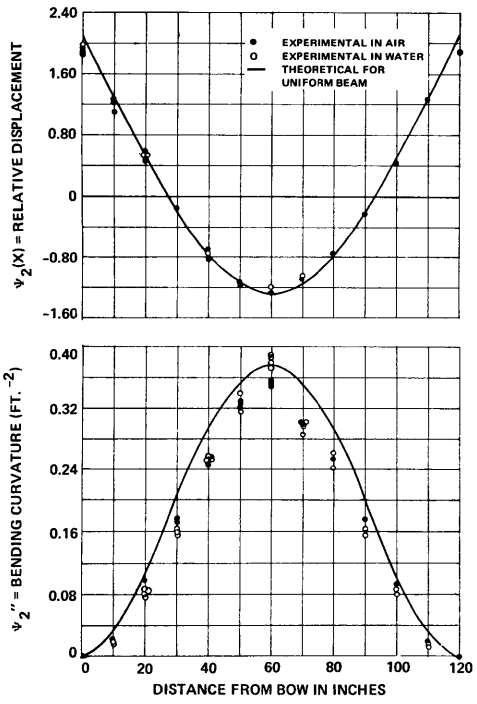

FIG. 5. Fundamental flexure mode of box target in air and in water.

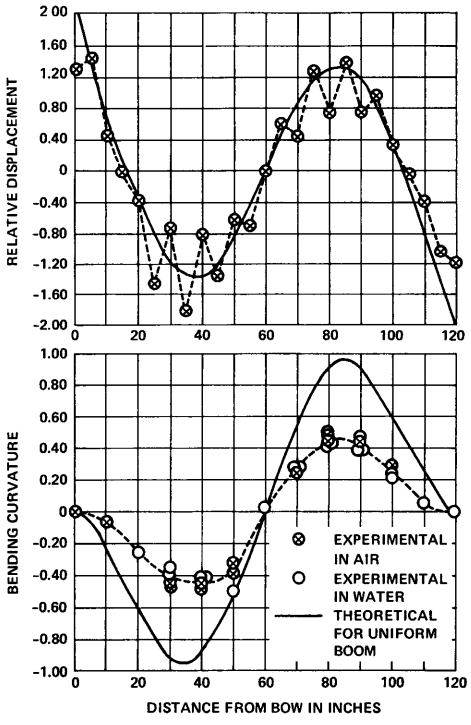

FIG. 6. Three-noded flexure mode of box target in air and in water.

mode of the box target. There is good agreement between the measurements in air and those in water, but all the measured deflections tend to oscillate about the theoretical values with a period equal to the distance between transverse frames in the box. The measured bending strains are only about half the theoretical values for a uniform bar which vibrates in the same mode with the same deflection amplitude. More comprehensive measurements made with a probe-type accelerometer showed a very large variation in amplitude (as much as 500%) at any one section. The amplitudes were least at the four corners, and in the neighborhood of stiffeners, bulkheads, and ballast weights.

Measurements were also made of the heaving and pitching frequencies, and of the mode shape and frequency of the ψ_4 mode. All of these frequency data were used to calculate virtual masses L_{ii} to compare with theoretical estimates of this quantity.[2] An important consequence of the mode-shape measurements is that the mode shapes in water are sensibly the same as in air, and therefore Eq. 13 for the position factor should be applicable.

B. Submerged Cylindrical Shell

The cylinder target was 99 in. long and 8.12 in. in diameter, with rib stiffeners, as shown in Fig. 7. The two end-plate covers weighed 19 lb, while the total weight was 80 lb, so that the target was markedly nonuniform along its length. Since there was no internal ballast, the total weight was only about 80% of the displacement. In this target, there were only 14 strain gauges to measure the bending strain at seven different sections of the target. The amplifying and recording equipment was the same as for the box target.

An effective vibration generator, which could be mounted on a cover plate and sealed within the target, was made from a 4-in. radio speaker in which the diaphragm had been replaced by a brass weight. Figure 8 shows the relative displacement and relative bending strains along the length of the cylinder for the ψ_2 and ψ_3 modes in air. The mode shape for bending strain in water was measured and found to be appreciably different than in air. This means that the distribution of inertial loading due to the virtual mass of water is appreciably different from the distribution of mass loading in the cylinder, and so Eq. 13 for the position factor may not be applicable.

Accordingly, for this cylinder target, the position factor was determined by a reciprocity measurement that was completely independent of the explosion tests. The cylinder was vibrated in the water at its resonance frequency with a constant vibration amplitude and the sound pressure distribution in the water was measured with a hydrophone. The position factor at point **r** is proportional to the resonance-frequency component of the sound pressure at point **r**. Since the hydrophone was

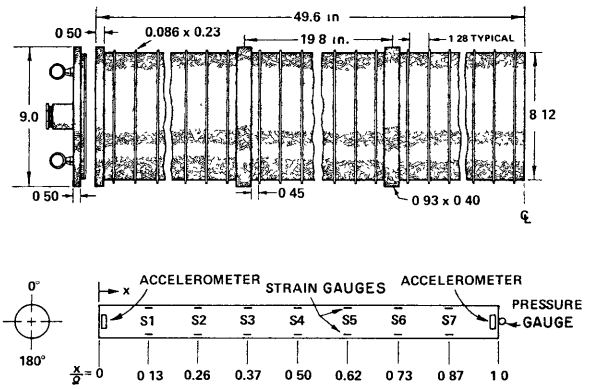

FIG. 7. Section of cylinder target showing locations of instrumentation.

not accurately calibrated at this frequency, the proportionality factor was determined by calculating the position factor for a field point off the midsection where Eq. 13 should be accurate.

C. The Explosion Bubble and Explosion Pressure

Experiments were made to determine and verify the bubble volume as a function of time, and, independently, the acceleration of the bubble volume versus time for the sizes of explosive charges used in the subsequent tests. The volume versus time behavior was determined by photographing the bubble action at 2500 frames per second when a commercial No. 8 detonator was fired at

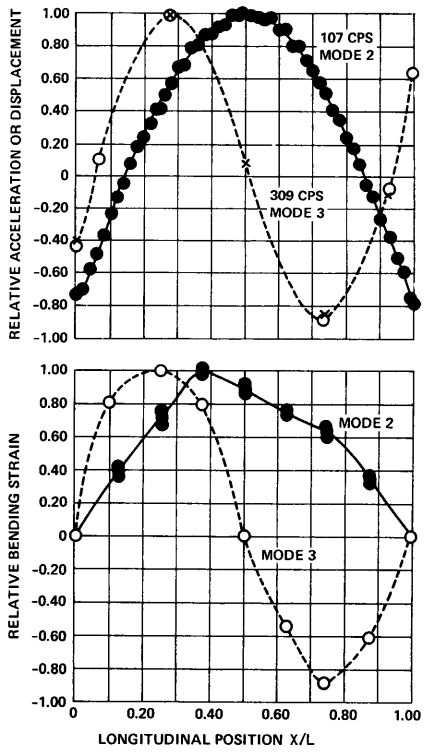

FIG. 8. Lowest flexural modes of cylinder target in air.

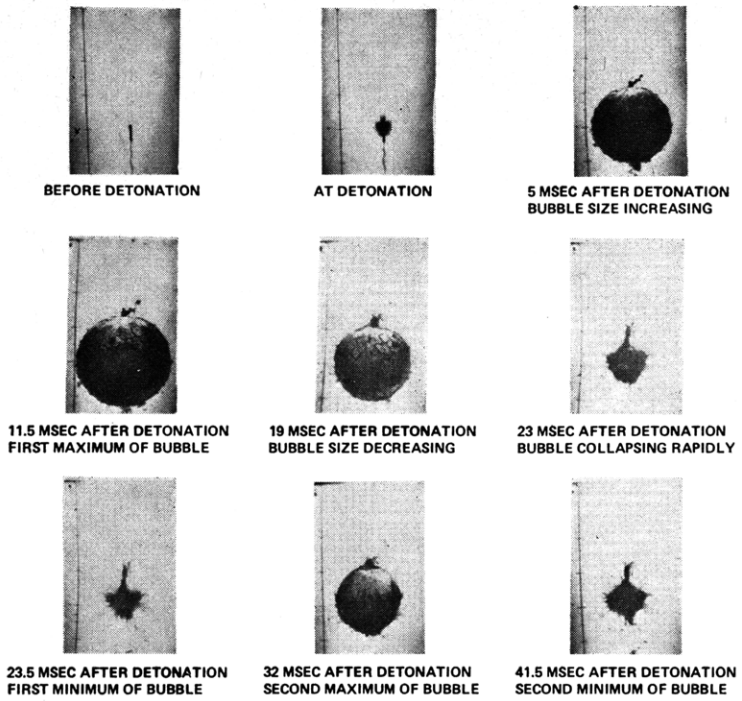

FIG. 9. Selected frames from high-speed photographs of explosion bubble under floating target.

13 in. below the floating box. Figure 9 shows selected frames from the photographs. The maximum bubble diameter was 10.8 in., and the first oscillation period was 23.5 msec. The entire history of the bubble volume fits the general curve for V/V_m vs t/T_b shown in Fig. 2. This curve had been constructed from these photographic measurements plus some theoretical analysis, plus many other bits of experimental data. An important result shown by the photographs is that, for these test conditions, the bubble retains an essentially spherical shape for more than two oscillation periods, and that during this interval the migration of the bubble is negligible. Similar photographs with the charge 12 in. below the box show that the bubble descends slightly at the first recompression; and, when the charge is 14 in. below the box, it rises slightly. An independent set of measurements of the transient pressure versus time at a fixed range from a pulsing explosion bubble confirmed that the transient pressures were equal to $\rho\ddot{V}/(4\pi r)$, except during the initial shock-wave phase, which was of too short a duration to be measured with the pressure gauges.

The $V(t)$ relation for the different charges and different depths used in the submerged cylinder tests was assumed to be the same as in Fig. 2 and Eqs. 2 and 3. The parameters for these equations were deduced from independent photographic measurements of V_m and T_b for each charge size at a depth of 10 ft.

D. Procedures for Measuring Normal Coordinates

The strain-gauge bridges in each target directly measure the instantaneous values of the local bending strains $\epsilon(x,t)$. Each bending strain is a superposition of strains due to the simultaneous action of all the bending modes of target vibration, i.e.,

$$\epsilon(x,t)=\sum_{i=2}^{\infty} q_i(t)\epsilon_i(x), \tag{16}$$

where $\epsilon_i(x)$ is the distribution of bending strain in mode i as measured in the lower modes by the vibration generator tests of the targets, and $q_i(t)$ is the normal coordinate for mode i and is the quantity we wish to deduce from the explosion response measurement for comparison with the theory. This was done by three different methods.

In the earliest tests with the box target, $\epsilon(x,t)$ was separately recorded at 11 different sections x, and thence $q_i(t)$ was calculated by a numerical integration

$$q_i(t)=\left[\int_0^l \epsilon(x,t)\epsilon_i(x)dx\right]\Big/\left(\int_0^l \epsilon_i^2 dx\right). \tag{17}$$

This equation can be obtained by multiplying Eq. 16 by $\epsilon_i(x)$ and integrating. It presupposes that the modal strain functions $\epsilon_i(x)$ form an orthogonal set. This is certainly true for the lower modes of the box model, because they closely resemble the modes for a uniform rod.

A second method of calculating q_i depends upon the realization that only a very few of the bending modes (say four) are appreciably excited. Hence, if experimental bending strain measurements are available at

any four sections $x=x_1, x_2, x_3, x_4$, then

$$\epsilon(x_i,t)=\sum_{j=2}^{5} q_j(t)\epsilon_j(x_i), \quad i=1, 2, 3, 4, \tag{18}$$

and

$$q_i(t)=\sum_{j=1}^{4} \frac{\epsilon^{ij}}{|\epsilon_i(x_j)|}\epsilon(x_j,t), \quad i=2, 3, 4, 5, \tag{19}$$

where $|\epsilon_i(x_j)|$ means the determinant of the coefficients $\epsilon_i(x_j)$, and ϵ^{ij} is the cofactor of the ij term in this determinant. This equation was used to compute $q_2(t)$ and $q_3(t)$ for the early tests with the box target. In the later tests, this same calculation was performed by a real-time-computing network during each test. Since the output circuits of the carrier amplifiers were not grounded, it was feasible not only to record each channel separately, but simultaneously to form particular linear combinations of the outputs according to Eq. 19 and record $q_2(t)$ and $q_3(t)$ directly.

In the explosion tests with the cylinder target, the bending strains at different sections were not recorded separately. Instead, the strain-gauge bridges for several sections (2, 3, or 4) were wired into a single bridge, which formed a linear combination of the bending strains according to Eq. 19. The single signal from this complex bridge circuit was then amplified and recorded as a direct real-time measurement of the normal coordinate $q_2(t)$ or $q_3(t)$.

E. Explosion Tests to Measure $q_2(t)$

Most of the explosion tests against the floating box target were made with a commercial No. 8 detonator (equivalent to about 1.2 g of TNT) at a depth of 15.6 in. below the water surface (13 in. below the bottom of the box). Since the charge size and depth were unchanged in these tests, then, according to Eq. 14, all measurements of the same normal coordinate $q_2(t)$ should have the same time pattern—only the amplitude should change in proportion to the position factor $\mu(\mathbf{r})$.

Figure 10 compares measured values of $q_2(t)$ in these tests with theoretical calculations. Curve C shows the values of $q_2(t)$ measured in a single test with the charge 13 in. below the center point of the bottom of the box. Curve D is the weighted average of measurements made in seven different tests, with the charge in a different longitudinal position for each test. The weighting factor is the ratio of the peak displacements for the first 80 msec in the test of Curve C to the same peak displacements in each test. Curves A and B are theoretical calculations for the same conditions as Curve C. Curve A was calculated by a numerical solution of the differential equation, Eq. 14, with the bubble volume acceleration $\ddot{V}(t)$ deduced from the pressure measurements. Curve B was calculated by a numerical solution of the integral equation, Eq. 15, with $V(t)$ deduced from the bubble photographs. Curve D should be more accurate

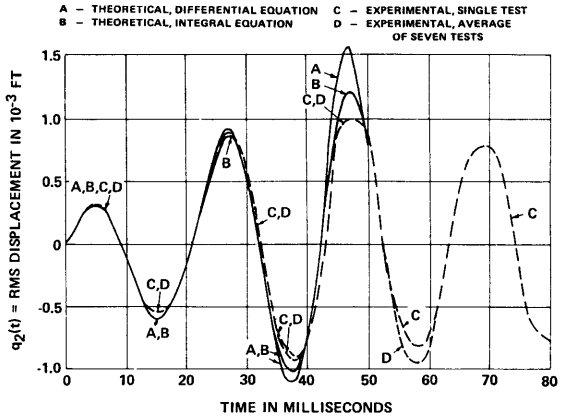

FIG. 10. Measured and theoretical values for $q_2(t)$ in explosion tests against floating target.

than C because the bubble volume is easier to measure than the pressure, and because the integral equation is easier to solve than the differential equation.

The close agreement between the two experimental Curves C and D confirms the theoretical expectation that the time pattern of the response depends only on the ratio of bubble period to modal vibration period, and the bubble period depends on the size and depth of the explosive. In Fig. 10, the first swing of the target is due to the initial shock wave. The amplitude is then increased by half on the reverse swing because of the underpressure phase of the explosion pressures (see Fig. 2); it is then pushed to three times its initial peak by the first bubble pulse, and the second pulse increases it still further. These features are all predicted by the theory in excellent quantitative agreement with the measurements. Incidentally, they also illustrate the fact that the low-amplitude–long-duration bubble pressures can have more influence than the high-amplitude–short-duration shock wave.

The data of Figs. 11 and 12 verify the theory of the position factor for a wide range of charge positions, the former for positions under the midsection to a point

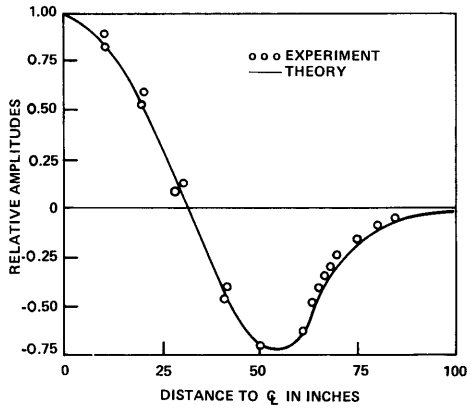

FIG. 11. Variation of whipping amplitudes of floating target with longitudinal position of explosion.

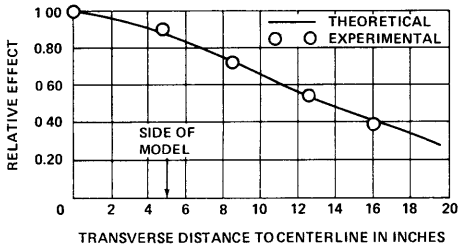

FIG. 12. Variation of whipping amplitudes of floating target with transverse position of explosion.

2 ft beyond the end of the box, and the latter for positions under the midsection to a point 1 ft beyond the side of the box. In both cases, the line curves are theoretical values calculated from Eq. 13, and the points are experimental values obtained by averaging the absolute value of $q_2(t)$ for 80 msec.

F. Explosion Tests Against Cylinder Target

The tests with the cylinder target were made to verify how the response varies with the size and depth of explosive. In these tests, the explosive was either

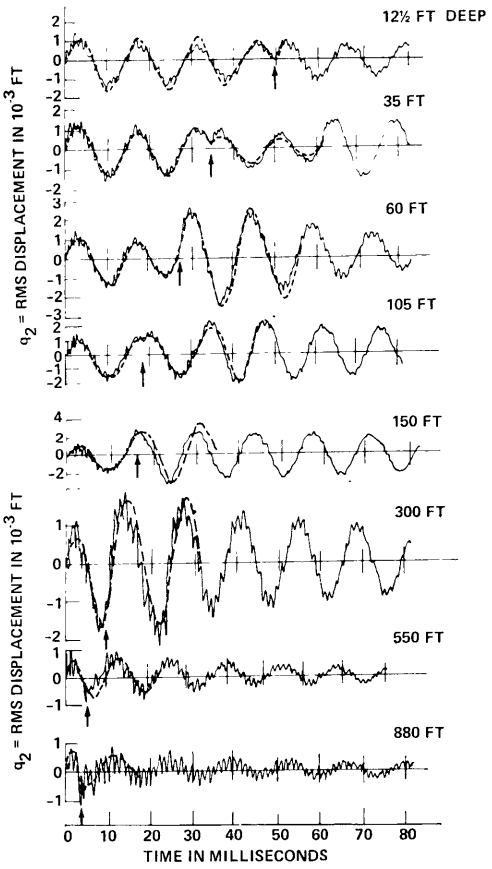

FIG. 13. Measurements of $q_2(t)$ during tests against submerged target at various depths with 8.2-g charge and 5-ft standoff. The dashed line shows the theoretical predictions; the arrow points to the bubble pulse.

1.2, 4.2, or 8.2 g, the depth of target and explosive together varied from 12 to 900 ft, and the standoff of charge from target varied from 1 to 5 ft. The target was suspended with its longitudinal axis in the vertical position in a harness which freely permitted small motions in the transverse direction and was kept submerged against its own buoyancy by an external ballast weight.

Figure 13 shows measurements of $q_2(t)$ made during eight different tests at depths from 12.5 to 880 ft. For these tests, the charge was 8.2 g placed 5 ft from the target axis in the plane of the midsection. The solid-line curves are direct tracings of the oscillograms in each test. The dashed-line curves are the theoretical predictions based upon a numerical solution of Eq. 15, with the position factor deduced from the reciprocity measurements, and with the $V(t)$ relation deduced from Fig. 2 and Eqs. 2 and 3. The arrow in each graph points to the time of the bubble pulse $t=T_b$. Figure 14 shows a similar comparison between experiment and theory for a series of explosion tests using a 1.2-g charge at 24 in. from the target axis.

As the test depth increases, the peak bubble volume decreases and tends to decrease the peak response. However, the bubble period also decreases with depth, causing the target vibration to vary its phase relative to the bubble oscillation. This phasing effect dominates the magnitude and pattern of the target response. Thus, in the two shallow tests in Fig. 13, the bubble pulse hits the target out of phase with the modal velocity and actually reverses the velocity. In the 60-ft test in Fig. 13, and the $12\frac{1}{2}$- and 60-ft tests in Fig. 14, the bubble pulse hits the target in phase with the target velocity and substantially reinforces the motion. In the 150- and 300-ft tests in Figs. 13 and 14, the first bubble pulse approximately synchronizes with zero target velocity and thus has little effect on the subsequent motion. Again, these features are all predicted by the theory in excellent agreement with the experiments.

There are some experimental results that are not predicted by the theory but can easily be explained qualitatively. One is the gradual decay in amplitude due to energy losses—about 5% to 10% per oscillation. This could be incorporated into the equation of motion as an ad hoc damping term, but, for the first two bubble oscillations, its effect is of the same order as the reproducibility in the experiments, and for later times its effect is of the same order as our uncertainty in the $V(t)$ curve for the bubble. On many of the oscillograms, there appear high-frequency signals with frequencies from 500 to 1000 cps which are not faithfully recorded because the amplifier and recorder response drops sharply above 400 cps. These signals are due to vibration modes other than the ψ_2 mode, probably axial vibration modes.

Figure 15 shows an interesting verification of the reciprocity theorem for charge position along a line

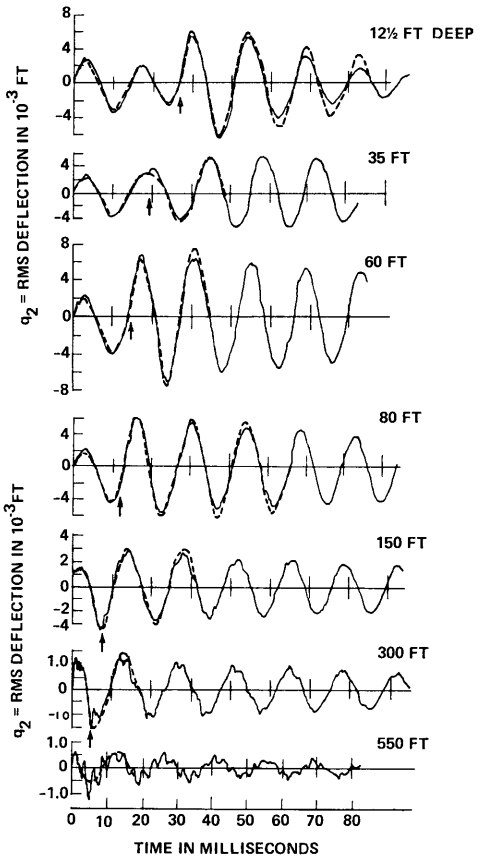

FIG. 14. Measurements of $q_2(t)$ during tests against submerged target at various depths with 1.2-g charge and 2-ft standoff. The dashed lines show the theoretical predictions; the arrow points to the bubble pulse.

parallel to the longitudinal axis. It compares relative values of the position factor which were determined in three ways: (1) by measuring the relative response in explosion tests, (2) by measuring the sound pressure at the field point due to steady vibration of the target excited by a vibration generator, and (3) by calculation from Eq. 13. Clearly, the two sets of measurements are in good agreement thus verifying the reciprocity theorem. But the theoretical values increasingly diverge from the measured values as the field point approaches the end of the target where the heavy end plates accentuate the nonuniformity in the target, thus verifying that Eq. 13 is not sufficiently accurate for this nonuniform target.

G. Measurement and Theory in Mode 3

The response to underwater explosives in the ψ_3 mode (three-noded flexure) was measured for both the floating box and submerged cylinder targets. The methods of measuring $q_3(t)$ were the same as for $q_2(t)$ except that the strain-gauge bridge circuit was adjusted to fit the parameters for ψ_3 in Eq. 19. Figure 16 shows the results of five different tests against the floating box with no

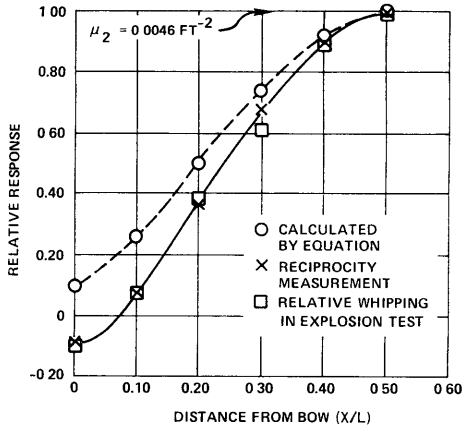

FIG. 15. Relative values of position factor $\mu_i(\mathbf{r})$ determined by three different methods.

change in the charge size or the charge depth but with different longitudinal positions. Note that the theoretical curves have the same pattern as the experimental curves, but that the theoretical amplitudes are about 30% too high. Figure 17 shows the results of tests against the submerged cylinder in mode 3 at six different depths. In this case, the measured amplitudes are larger than the theoretical predictions. In the box target, it was known that the deflections in mode 3 are a complex function of position. They are not uniform across any section and they are not related to the strains in the bridge circuit in any simple way. For the cylinder target, it also appears as though the bridge circuit for mode 3 was not sufficiently selective and that other vibration modes influence the response.

IV. SUMMARY AND CONCLUDING REMARKS

(1) The flexural response of a ship-like target to a nearby underwater explosion is analyzed in terms of the

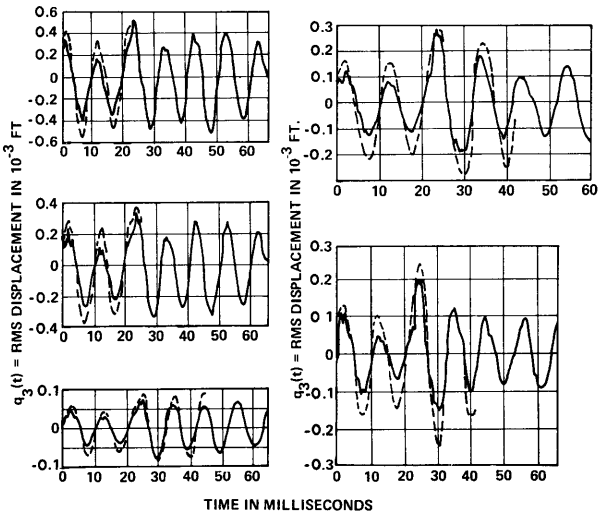

FIG. 16. Measurements (——) and theoretical calculations (– – –) of $q_3(t)$ for the tests against floating target with charge in different longitudinal positions.

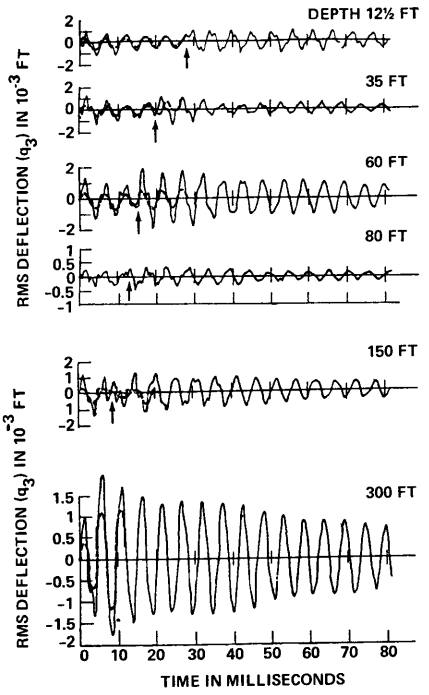

FIG. 17. Measurements (——) and theoretical calculations (– – –) of $q_3(t)$ for tests against submerged target at various depths.

independent contributions from the principal, or normal, modes of the structure and entrained water. The use of normal-mode theory presupposes that the motions are linear and elastic and that no plastic deformations occur. The use of normal modes for the combined system of structure and water further presumes that only low-frequency motions of the structure are considered, so that the water can be treated as incompressible.

(2) Each principal vertical flexural mode of the system responds to the explosive forces like a line distribution of vertical dipoles with a prescribed dipole strength (Eq. 14). Essentially, this is a consequence of the slender shape of the body.

(3) The generalized force for each principal mode varies with time in proportion to the volume acceleration of the explosion bubble. This includes the forces due to the initial shock wave and the subsequent bubble oscillation but omits the force due to any migration of the bubble. The assumed behavior of the bubble was verified by independent measurements of the bubble volume with time, and by independent measurements of the pressures in the water.

(4) The instantaneous modal force on the target varies with the position of the explosion in proportion to the instantaneous sound pressure which would be generated at that position by a steady vibration of the structure at the resonance frequency for that mode. This reciprocity theorem was verified by sound-pressure measurements during an independent series of steady-state vibrations of the structure with a vibration generator.

(5) The theoretical predictions of the transient motion in a single mode were verified by experiments with small charges against a floating or submerged target. Direct real-time measurements were made of the normal coordinates for two different flexural modes. The modal parameters for the theoretical predictions in these tests were deduced from an independent series of steady-vibration measurements.

ACKNOWLEDGMENT

This review is based on David Taylor Model Basin Technical Reports originally written by the author in association with T. F. Ogilvie, A. Hirsch, R. Mayo, and J. Lax, to each of whom he acknowledges his indebtedness.

[1] G. Chertock, J. Appl. Phys. **24**, 192–197 (1953); see also David Taylor Model Basin Report C-157 (Oct. 1952).
[2] G. Chertock, A. E. Hirsch, and T. F. Ogilvie, David Taylor Model Basin Report C-159 (Feb. 1953).
[3] G. Chertock, J. Acoust. Soc. Amer. **34**, 989(L) (1962).
[4] G. Chertock, J. Acoust. Soc. Amer. **36**, 1305–1313 (1964).

INITIAL DISTRIBUTION

Copies

2 NAVMAT
- 1 MAT 03L4
- 1 MAT 03L4A

6 NAVSEC
- 3 SEC 6105B
- 3 SEC 6105C

4 NAVSHIPSYSCOM
- 1 SHIPS 031
- 1 SHIPS 0341
- 1 SHIPS 035
- 1 SHIPS 03423

2 CHONR
- 1 Code 466
- 1 Code 468

20 CDR, DDC

UNCLASSIFIED
Security Classification

DOCUMENT CONTROL DATA - R & D

(Security classification of title, body of abstract and indexing annotation must be entered when the overall report is classified)

1 ORIGINATING ACTIVITY (Corporate author)	2a. REPORT SECURITY CLASSIFICATION
Naval Ship Research and Development Center Washington, D.C. 20034	UNCLASSIFIED
	2b. GROUP

3 REPORT TITLE

TRANSIENT FLEXURAL VIBRATIONS OF SHIP-LIKE STRUCTURES EXPOSED TO UNDERWATER EXPLOSIONS

4 DESCRIPTIVE NOTES *(Type of report and inclusive dates)*

Reprint from Journal of Acoustical Society of America

5 AUTHOR(S) *(First name, middle initial, last name)*

George Chertock

6 REPORT DATE	7a. TOTAL NO OF PAGES	7b. NO OF REFS
Oct 1970	11	4

8a. CONTRACT OR GRANT NO	9a. ORIGINATOR'S REPORT NUMBER(S)
b. PROJECT NO. R11-01	3504
c.	9b. OTHER REPORT NO(S) *(Any other numbers that may be assigned this report)*
d	

10 DISTRIBUTION STATEMENT

This document has been approved for public release and sale; its distribution is unlimited.

11 SUPPLEMENTARY NOTES	12 SPONSORING MILITARY ACTIVITY
	NAVMAT

13 ABSTRACT

The flexural vibrations of ship-like structures are easily excited by underwater explosions, particularly if the explosion bubble period approximately synchronizes with a period of flexural vibration. A summary of the theoretical analysis shows how the transient motions are related to the principal vibration modes of the structure, and to the distribution and history of the applied pressures. The latter depend on the size, depth, and relative position of the explosive. Experiments on small idealized ship and submarine models are described which vary the weight, depth, and position of the explosive, and which measure the instantaneous deformations of the structure with strain gauges connected into special bridge circuits to yield the normal coordinates associated with the principal flexural vibration modes. Comparison of the theory and experiments verify the theory as applied to the fundamental flexural mode, and with less precision, as applied to the higher flexural modes. The principal mode patterns and the history of the explosion bubble are verified by independent experiments.

14 KEY WORDS	LINK A		LINK B		LINK C	
	ROLE	WT	ROLE	WT	ROLE	WT
TRANSIENT VIBRATIONS						
UNDERWATER EXPLOSIONS						
SHIP MOTIONS						